On nonlinear model predictive direct yaw moment control for trailer sway mitigation

Taylor & Francis
Taylor & Francis Group

Vehicle System Dynamics
International Journal of Vehicle Mechanics and Mobility

ISSN: (Print) (Online) Journal homepage: www.tandfonline.com/journals/nvsd20

On nonlinear model predictive direct yaw moment control for trailer sway mitigation

Martino De Bernardis, Gabriele Rini, Francesco Bottiglione, Ahu Ece Hartavi & Aldo Sorniotti

To cite this article: Martino De Bernardis, Gabriele Rini, Francesco Bottiglione, Ahu Ece Hartavi & Aldo Sorniotti (2023) On nonlinear model predictive direct yaw moment control for trailer sway mitigation, Vehicle System Dynamics, 61:2, 445-471, DOI: 10.1080/00423114.2022.2054352

To link to this article: https://doi.org/10.1080/00423114.2022.2054352

Published online: 09 Aug 2022.

VEHICLE SYSTEM DYNAMICS
2023, VOL. 61, NO. 2, 445–471
https://doi.org/10.1080/00423114.2022.2054352

IAVSD
Taylor & Francis
Taylor & Francis Group

RESEARCH ARTICLE
OPEN ACCESS
Check for updates

On nonlinear model predictive direct yaw moment control for trailer sway mitigation

Martino De Bernardis[a], Gabriele Rini[a,b], Francesco Bottiglione[b], Ahu Ece Hartavi[a] and Aldo Sorniotti[a]

[a]Centre for Automotive Engineering, University of Surrey, Guildford, UK; [b]Dipartimento di Meccanica, Matematica e Management, Politecnico di Bari, Bari, Italy

ABSTRACT

In car–trailer combinations, the hitch angle is the relative yaw angle between towing car and trailer. The literature has shown that the inclusion of the hitch angle measurement for the feedback control of trailer oscillations can bring safety benefits, compared with conventional trailer sway mitigation algorithms based on the yaw rate of the car. Given the nonlinearity of the vehicle system in the typical conditions requiring the hitch angle control function intervention, nonlinear model-based controllers could be an effective solution. This paper presents four real-time implementable nonlinear model predictive control (NMPC) formulations, using the hitch angle measurement for the torque-vectoring (TV) control of an electric front-wheel drive car towing a trailer. The simulation results show that: (i) the active safety is enhanced by the proposed NMPC TV formulations, with respect to a benchmarking NMPC TV controller only based on the control of the towing car; (ii) the NMPC formulations that directly constrain the hitch angle error, or perform continuous hitch angle tracking, outperform those that modify the reference yaw rate or yaw rate error based on the hitch angle error; and (iii) the NMPC approaches including a dynamic model of the trailer are robust with respect to variations of trailer parameters.

ARTICLE HISTORY
Received 30 June 2021
Revised 28 October 2021
Accepted 26 February 2022

KEYWORDS
Car-trailer combination; trailer sway; hitch angle; nonlinear model predictive control; torque-vectoring; performance comparison

1. Introduction

The response of car–trailer systems in high-speed conditions can be affected by significant oscillations and stability issues, which are very difficult to control also for experienced drivers, and cause safety-critical scenarios. For example, depending on the vehicle parameters and operating conditions, car–trailer systems can become prone to jackknifing and snaking. The insurgence of the hitch angle dynamics is facilitated by specific sets of trailer parameters, which vary with the payload. The dominant factors affecting lateral stability are the trailer yaw mass moment of inertia, the longitudinal position of the trailer centre of gravity, the location of the hitch joint, and the position of the trailer axle/s, while the trailer mass alone does not significantly affect high-speed stability [1].

CONTACT Aldo Sorniotti a.sorniotti@surrey.ac.uk

Trailer oscillations can be mitigated through appropriate controllers. Several studies from the literature apply the control action only to the towing vehicle. For example, in Gerum et al. [2] braking torques are generated on the rear wheels of the tractor, to produce the direct yaw moment computed by an adaptive controller supported by an adaptive observer for hitch angle and hitch rate estimation. In [3] Mokhiamar and Abe propose two sliding mode formulations for direct yaw moment control, one based on the sideslip angle and the other one on the yaw rate of the towing vehicle. In [4] Deng and Kang compare multiple feedback controllers, which, starting from the hitch angle and hitch rate of the trailer, or on the yaw rate and lateral velocity of the towing vehicle, or the combination of the previous variables, generate a reference steering angle for the rear wheels of the car.

Other authors only consider actuators located on the trailer. In this respect, in [5] Fernández and Sharp use the measured hitch angle and its time derivative to calculate asymmetric braking pressure demands for a caravan, to limit its sway. In [6] Plöchl et al. propose a sliding mode controller that calculates a corrective direct yaw moment actuated by the trailer brakes, starting from the yaw rates of the trailer and tractor. In [7] Sun et al. investigate an active trailer differential braking controller based on a linear quadratic regulator (LQR) and highlight that its integration with an active car differential braking controller would further improve the lateral stability of the car–trailer combination. In [8] Shamim et al. compare three stability control methods for car–trailer systems, namely active trailer braking, active trailer steering, and a variable geometry approach based on the active control of the lateral displacement of the car–trailer hitch joint. The results show that active trailer braking control has the best capability of rejecting external disturbances and maintaining stable operation of the car–trailer combination at high speeds. In [9] MacAdam et al. discuss a simple brake control algorithm to reduce the rearward amplification (RWA) in doubles and triples combination trucks, with a modular layout that can be implemented on a trailer-by-trailer basis. In [10] Milani et al. propose three LQR formulations to improve articulated heavy vehicle (AHV) manoeuvrability and stability through active semitrailer steering and anti-roll control, where the state feedback is based on the roll angle, roll rates, yaw rates and sideslip angles of the vehicle units. In [11] Tabatabaei Oreh et al. discuss an active steering system for the trailer, based on fuzzy logic control, to track a reference hitch angle based on a novel formulation. References [12] and [13] deal with active trailer steering controllers for AHVs, based on LQRs including hitch angle feedback. In [14] the LQR approach, in this case based on state feedback using the yaw rate and lateral slip speed of each vehicle unit, is robustified through the implementation of a linear-matrix-inequality-based method. Islam et al. [15] present a parallel design optimisation method for AHVs with active safety systems, which simultaneously optimises the active design variables of the controllers and passive design variables of the trailers in a single loop.

A few studies compare actuation solutions located on the towing vehicle, the trailer, or both. One of the main conclusions is that if the dynamic coupling between the towing vehicle and trailer is weak, then a leading unit based controller may not be effective to suppress violent trailer oscillations in critical conditions [16]. However, this does not have general validity. For example, Abroshan et al. [17] present a model predictive controller (MPC) for the yaw stabilisation of an articulated vehicle capable of differential braking actuated either on the trailer or the tractor, where the latter – for the specific vehicle – is the more effective solution. This outcome is confirmed by Zhang et al. [18], who propose

a reconfigurable MPC architecture for articulated vehicle stabilisation, which is tested on an electrified car–trailer combination capable of multiple direct yaw moment generation options. In [19] Wang et al. highlight the benefits of the concurrent control of tractor and trailer, with respect to the control of the individual units, by applying a proportional integral derivative (PID) direct yaw moment controller to a single-track articulated vehicle model.

The current industrial solution adopted in the stability controllers of passenger cars is to include trailer sway mitigation algorithms without any dedicated system to measure or estimate the hitch angle or yaw rate of the trailer [20,21]. According to this approach, the yaw rate error of the car is subjected to band-pass filtering to obtain a signal in the typical frequency range of the trailer resonance. When this variable exceeds a threshold, critical trailer behaviour can be inferred, and appropriate control action is applied through the braking system of the car [22]. While the method can be effective in addressing the persistent oscillations of snaking at high speed, its benefits are very limited in the compensation of trailer sway caused by extreme transient steering applications, e.g. typical of obstacle avoidance or emergency manoeuvring. A simple yet effective commercially available solution is represented by the ATC system by AL-KO [23], which provides emergency braking functionality to the trailer, and is activated automatically if the vehicle combination experiences stability issues, i.e. if the swinging of the trailer reaches a critical level.

The simulation and experimental analysis in [24] compares a conventional yaw rate based commercial trailer sway mitigation algorithm with a feedback control formulation correcting the yaw rate error with a hitch angle error contribution in case of major trailer oscillations in car–trailer combinations. The results show the potentially significant active safety benefits of direct hitch angle control, with respect to the production yaw rate focused strategies. Moreover, as the recent literature discusses several methods for hitch angle estimation or measurement, e.g. through model-based techniques or ultra-sonic sensors or vision systems located on the rear end of the towing vehicle [25–31], the additional complexity related to the on-board acquisition of the hitch angle information could soon become industrially viable.

While in production passenger cars the trailer sway control function is actuated through the friction brakes, in next generation electric vehicles with multiple motors, the corrective direct yaw moment could be implemented through individual motor control, i.e. through torque-vectoring (TV) [24], thus providing enhanced tracking performance and progressivity as well as reduced power losses.

MPC is gaining increasing attention for advanced vehicle dynamics control. For example, the path tracking controller of the automated articulated agricultural vehicle in [32] uses a nonlinear kinematic model, and, although providing excellent results for the specific application, neglects the axle slip angles, which are of the essence in road vehicles for capturing the hitch angle dynamics in emergency conditions. In the context of trailer sway control, the available pioneering implementations in [17,18] and [33] are based on linear time-varying MPC, i.e. the internal vehicle model, and in particular its tyre model, is linearised at each time step, and its parametrisation is kept constant along the prediction horizon. This simplified prediction model is an extension of the well-known two-degree-of-freedom linear bicycle model for rigid vehicles. The benefit is a reduction of the computational effort for the solution of the optimal control problem, while still providing good vehicle stabilisation capability. The drawbacks are: (a) the potentially reduced

performance, as the control input is expressed in terms of reference yaw moment, and therefore the prediction model does not account for the interaction between longitudinal and lateral tyre forces, see also the analysis in [34] on the significance of the internal model features on stability control performance in rigid vehicles; (b) the exclusion of the wheel dynamics from the internal model formulation, which does not allow the implementation of integrated wheel slip control; (c) the need for the continuous and precise information on the current value of the axle cornering stiffness, which implies additional estimation complexity, with respect to the estimation of the tangential tyre forces and slip angles; and (d) limitations with respect to the future development of MPC formulations considering longer prediction horizons, within which the linearisation approximation would not be reliable any longer. In fact, in the next generation of pre-emptive stability controllers for connected vehicles, see [35], the future steering inputs and reference state profiles, e.g. the reference yaw rate, could be approximately known a priori, and thus the extension of the prediction horizon would bring evident vehicle stabilisation improvements, provided that the internal model can accurately predict the vehicle system dynamics for the range of conditions within the selected horizon.

In summary, to the best of our knowledge, none of the previous studies proposes hitch angle controllers based on nonlinear model predictive control (NMPC) technology, which is becoming real-time implementable, see the examples in [36–38], thanks to the development of dedicated computationally efficient solvers [39], and the progressive improvement of automotive control hardware. This paper targets the identified gap, through the following contributions:

- Four NMPC formulations for an electric car with front individually controlled powertrains and towing a passive single-axle trailer, including continuous control of the yaw rate of the car as well as sideslip angle and hitch angle limitation in emergency conditions.
- The objective comparison of the performance of the proposed trailer sway mitigation algorithms with that of a benchmarking TV formulation designed for the control of the car on its own. All configurations are tuned through an optimisation routine, and assessed through an experimentally validated vehicle model.
- The assessment of the sensitivity of controller performance to the variation of the trailer parameters, without varying the controller or prediction model parameters.

The manuscript is organised as follows: Section 2 discusses the controller formulations; Section 3 describes the simulation environment, and the controller implementation and tuning details; Section 4 presents the controller comparison results; finally, Section 5 summarises the main conclusions.

2. Controllers formulations

2.1. Reference yaw rate and hitch angle

In the specific implementation of this study, for the control of the car yaw rate and hitch angle dynamics, in accordance with the common practices of vehicle stability control [40,41], the reference variables correspond to the steady-state cornering condition of the

vehicle, for the given driver inputs. The dynamic instability of the car–trailer combination is identified when the actual response significantly differs from the steady-state conditions.

The nonlinear map of the steady-state reference yaw rate of the towing car, $\dot{\psi}_{d,SS}$, is designed to match the steady-state cornering response of the passive (i.e. without TV) rigid vehicle, and is expressed as a function of steering angle, S_W, vehicle speed, V, and tyre-road friction coefficient, μ, see the extract in Figure 1. In the online implementation of the controller, $\dot{\psi}_{d,SS}$ is filtered through a first-order transfer function to obtain the car reference yaw rate, $\dot{\psi}_d$. It was verified that the controller can successfully operate even if the reference yaw rate for the car is not accounting for the interaction between trailer and car, which is, however, considered in the internal model described in the remainder for three of the proposed NMPC formulations, and through the hitch angle feedback. Figure 1 compares the steady-state yaw rate generated with the rigid vehicle, used as reference yaw rate for the car–trailer combination, and the actual steady-state yaw rate of the car–trailer combination, in case of trailer A (see Table 1 in Section 3.2). The presence of the trailer increases the vertical tyre load on the rear axle of the car, and transmits lateral and longitudinal forces to the towing vehicle through the hitch joint. The result is an increase of the corresponding rear axle slip angles, and thus a reduction of the level of vehicle understeer, with increased yaw rate values of the car for given S_W and V. However, the car yaw rate for the car–trailer combination is not significantly different from the yaw rate of the rigid vehicle, which means that the results presented in the remainder are acceptable. Moreover, it was verified through specific simulations that the inclusion of the reference yaw rate of the car–trailer combination would bring worse results in terms of hitch angle stability, given the marginally larger magnitude of the yaw rate of the combination vehicle. The conclusion is that the considered approximation is not only acceptable, but also safe and conservative. In the proposed formulations, the reference yaw rate mainly targets the control of the cornering behaviour of the car when the hitch angle dynamics are not critical, similarly to the operation of typical stability controllers or TV controllers for rigid vehicles, while the trailer sway mitigation function is mainly achieved through hitch angle feedback.

Similarly to [24], the reference hitch angle, θ_d, is obtained from the differential equation describing the hitch dynamics at constant V, under the assumption of kinematic steering conditions, i.e. with zero axle slip angles:

$$\dot{\theta} = \frac{V}{L_{TOT}} \left\{ \frac{L_{TOT}}{L_{TOT,T}} \sin(\theta) + \left[\frac{c - L_R}{L_{TOT}} \cos(\theta) + 1 \right] \tan(S_W) \right\} \tag{1}$$

where $\dot{\theta}$ is the time derivative of the hitch angle θ, defined as the angle between the longitudinal axes of the towing vehicle and trailer, see the schematic and nomenclature in Figure 2; L_{TOT} is the wheelbase of the towing car, while L_R is its rear semi-wheelbase; c is the longitudinal distance between the centre of gravity of the car (CG) and the hitch joint; and $L_{TOT,T}$ is the distance between the hinge and the rear axle of the trailer. By imposing $\dot{\theta} = 0$ in (1), θ_d is obtained as:

$$\theta_d = \tan^{-1} \left(\frac{\tan(S_W) \left\{ L_{TOT}^2 L_{TOT,T} + [c - L_R] \sqrt{\tan^2(S_W) L_{TOT}^2 [c - L_R]^2 - \tan^2(S_W) L_{TOT}^2 L_{TOT,T}^2 + L_{TOT}^4} \right\}}{L_{TOT} \left\{ -\tan^2(S_W) L_{TOT} [c - L_R] + \sqrt{\tan^2(S_W) L_{TOT}^2 [c - L_R]^2 - \tan^2(S_W) L_{TOT}^2 L_{TOT,T}^2 + L_{TOT}^4} \right\}} \right) \tag{2}$$

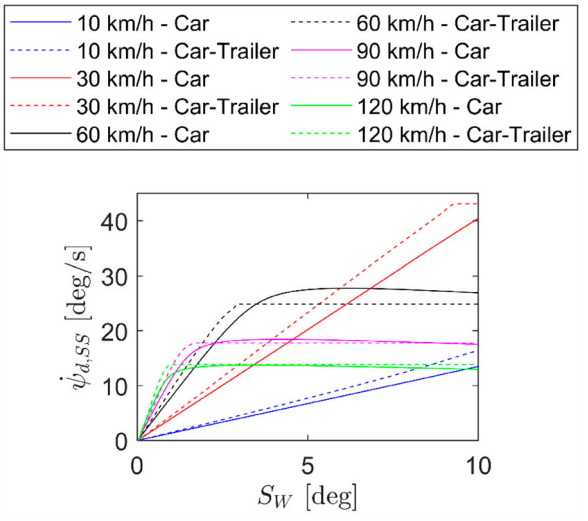

Figure 1. Steady-state yaw rate as a function of steering angle and vehicle speed, for high tyre-road friction conditions, obtained during ramp steer tests with the car (these profiles were used for the steady-state reference yaw rate map in the controller implementations of this study) and the car-trailer combination.

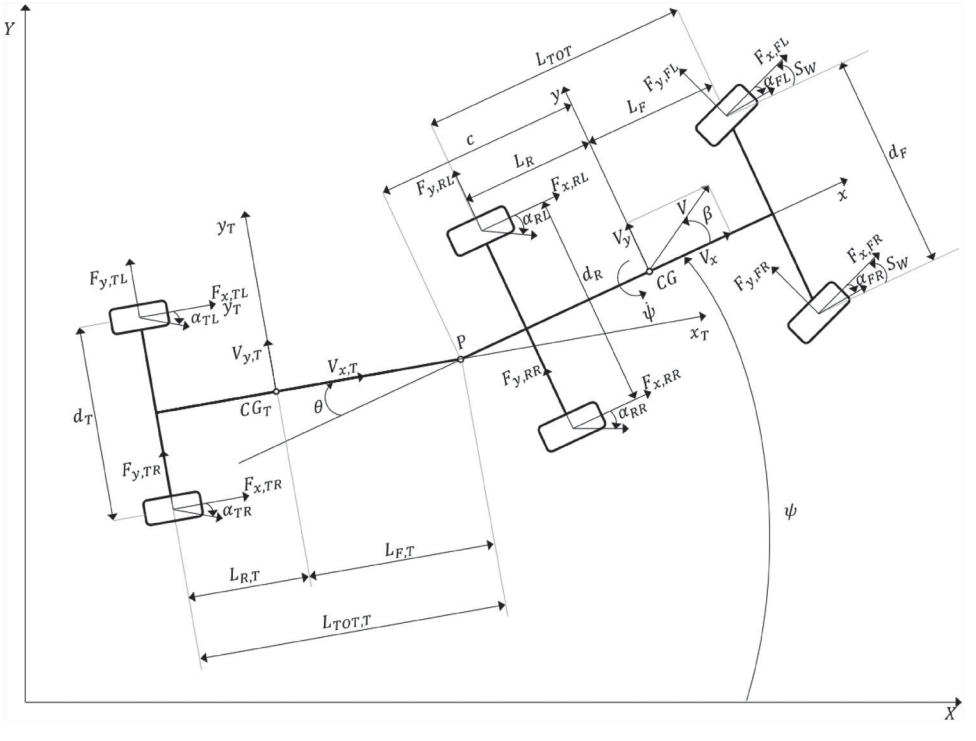

Figure 2. Simplified top view of the car-trailer system with the adopted nomenclature.

2.2. Internal model formulation

The equations of the car–trailer body dynamics of the NMPC internal model – also called prediction model – were obtained through the Lagrange method, which, in the specific case, is expressed through the formulation in [42], to obtain the system dynamics in the reference frame of the towing car (xy):

$$\frac{\partial}{\partial t}\left(\frac{\partial \mathrm{T}}{\partial w}\right) + A^T\left\{\dot{A} - \left[w^T A^T \frac{\partial A}{\partial q_l}\right]\right\}\frac{\partial \mathrm{T}}{\partial w} - A^T\frac{\partial \mathrm{T}}{\partial q_l} + \frac{\partial F}{\partial w} = A^T Q_l \tag{3}$$

where t is time; T is the kinetic energy of the system; $w = [V_x, V_y, \dot{\psi}, \dot{\theta}]^T$ is the vector of generalised velocities, in which V_x and V_y are the longitudinal and lateral components of the vehicle velocity V, and $\dot{\psi}$ is the car yaw rate; $F = 0.5\Gamma\dot{\theta}^2$ is the Rayleigh dissipation function, which is used to approximate viscous or friction effects in the hitch joint, with Γ being the damping coefficient of the hinge; q_l, with $l = 1, \ldots, 4$, indicates the individual generalised coordinates of the Lagrange formulation, which form the vector $q = [X_{CG}, Y_{CG}, \psi, \theta]^T$, with X_{CG} and Y_{CG} being the coordinates of the centre of gravity of the towing vehicle (i.e. the car) in the inertial reference frame; Q_l indicates the corresponding generalised forces, F_X and F_Y, in the inertial reference frame, and the moments related to the rotations ψ and θ; and A is the rotation matrix from the towing vehicle reference frame (xy) to the inertial reference frame (XY), such that $w = A^T\dot{q}$. According to this approach, the kinetic energy of the system can be expressed as a function of w:

$$\begin{aligned}\mathrm{T} = {} & \frac{1}{2}M[V_x^2 + V_y^2] + \frac{1}{2}J_1(\theta)\dot{\psi}^2 + \frac{1}{2}J_3\dot{\theta}^2 - J_2(\theta)\dot{\psi}\dot{\theta} - m_T V_y\{c\dot{\psi} + L_{F,T}[\dot{\psi} - \dot{\theta}]\cos(\theta)\} \\ & - m_T V_x L_{F,T}[\dot{\psi} - \dot{\theta}]\sin(\theta)\end{aligned} \tag{4}$$

where $M = m + m_T$ is the total mass of the vehicle-trailer combination; m_T is the mass of the trailer; $L_{F,T}$ is the distance between the hinge and the centre of gravity of the trailer; and $J_1(\theta)$, $J_2(\theta)$, and J_3 are equivalent mass moments of inertia, defined as:

$$J_1(\theta) = J_Z + J_T + m_T[L_{F,T}^2 + c^2 + 2L_{F,T}c\cos(\theta)] \tag{5}$$

$$J_2(\theta) = J_T + m_T[L_{F,T}^2 + L_{F,T}c\cos(\theta)] \tag{6}$$

$$J_3 = J_T + m_T L_{F,T}^2 \tag{7}$$

where J_Z and J_T are the yaw mass moments of inertia of the car and trailer.

The generalised forces and moments in the car reference frame, $A^T Q_l$, are obtained through D'Alembert's principle, according to which the total virtual work, δL, is defined as:

$$\delta L = \sum_n F_n \delta_{lin,n} + \sum_n M_n \delta_{ang,n} \tag{8}$$

where F_n and M_n indicate the virtual forces and moments; and $\delta_{lin,n}$ and $\delta_{ang,n}$ are the relevant components of the linear and angular displacements. The main sources of virtual work are the longitudinal and lateral tyre forces of the car and the trailer, which, in the remainder, are referred to as $F_{x,ij}$ and $F_{y,ij}$, where the subscript $i = F, R, T$ indicates the front or

rear axles of the car, or the trailer axle, and $j = L, R$ indicates the left or right vehicle sides. For the derivation of the virtual work, $F_{x,Fj}$ and $F_{y,Fj}$ are projected along the axes of the xy reference system of the car, according to the steering angle S_W, while, under the assumption of zero toe angle, $F_{x,Rj}$, $F_{y,Rj}$ $F_{x,Tj}$ and $F_{y,Tj}$ are already aligned with the axes of the coordinate systems of the respective vehicle, and therefore do not need any manipulation. The resulting forces are multiplied by the longitudinal and lateral virtual displacements of the car corners, δx_{ij} and δy_{ij}, and trailer corners, δx_{Tj} and δy_{Tj}, expressed in the respective vehicle unit reference frames:

$$\begin{cases} \delta x_{ij} = \delta x - y_{ij}\delta\psi, i = F, R \\ \delta y_{ij} = \delta y + x_{ij}\delta\psi, i = F, R \\ \delta x_{Tj} = \delta x\cos(\theta) - \delta y\sin(\theta) + c\delta\psi\,\sin(\theta) - y_{Tj}[\delta\psi - \delta\theta] \\ \delta y_{Tj} = \delta x\sin(\theta) + \delta y\cos(\theta) - c\delta\psi\,\cos(\theta) - L_{TOT,T}[\delta\psi - \delta\theta] \end{cases} \tag{9}$$

where the notation δ refers to a generic virtual displacement; x_{ij} and y_{ij} $(i = F, R)$ are the longitudinal and lateral coordinates of the ij wheel of the car, in the xy system; and y_{Tj} is the lateral coordinate of the j wheel of the trailer, in the $x_T y_T$ reference system. The tyre self-alignment moments are neglected in the prediction model formulations. The terms $A^T Q_l$ are obtained by differentiating the virtual work with respect to the virtual displacements δx, δy, $\delta\psi$ and $\delta\theta$:

$$A^T Q_l = \frac{\partial \delta L}{\partial \delta q_l} \tag{10}$$

The resulting equations of motion are:

- Longitudinal vehicle dynamics equation

$$\begin{aligned} &M\left[\dot{V}_x - \dot{\psi}V_y\right] - m_T L_{F,T}\left[\ddot{\psi} - \ddot{\theta}\right]\sin(\theta) - 2m_T L_{F,T}\dot{\psi}\dot{\theta}\cos(\theta) + m_T L_{F,T}\dot{\theta}^2\cos(\theta) \\ &\quad + m_T\dot{\psi}^2[c + L_{F,T}\cos(\theta)] \\ &= [F_{x,FL} + F_{x,FR}]\cos(S_W) - [F_{y,FL} + F_{y,FR}]\sin(S_W) + F_{x,RL} + F_{x,RR} \\ &\quad + \sum_{j=L,R}[F_{x,Tj}\cos(\theta) + F_{y,Tj}\sin(\theta)] - F_{drag} \end{aligned} \tag{11}$$

  where the term F_{drag} is the equivalent aerodynamic drag force of the vehicle combination, for simplicity considered along the longitudinal axis of the car.
- Lateral vehicle dynamics equation

$$\begin{aligned} &M\left[\dot{V}_y + \dot{\psi}V_x\right] - m_T\ddot{\psi}[c + L_{F,T}\cos(\theta)] + m_T L_{F,T}\ddot{\theta}\cos(\theta) - m_T L_{F,T}\sin(\theta)[\dot{\psi} - \dot{\theta}]^2 \\ &\quad = [F_{x,FL} + F_{x,FR}]\sin(S_W) + [F_{y,FL} + F_{y,FR}]\cos(S_W) + [F_{y,RL} + F_{y,RR}] \\ &\quad + \sum_{j=L,R}[-F_{x,Tj}\sin(\theta) + F_{y,Tj}\cos(\theta)] \end{aligned} \tag{12}$$

- Yaw dynamics equation

$$\begin{aligned} &J_1(\theta)\ddot{\psi} - J_2(\theta)\ddot{\theta} + m_T L_{F,T} c\sin(\theta)[\dot{\theta}^2 - 2\dot{\theta}\dot{\psi}] - m_T L_{F,T}\sin(\theta)\left[\dot{V}_x - V_y\dot{\psi}\right] \\ &\quad - m_T\left[\dot{V}_y + V_x\dot{\psi}\right][c + L_{F,T}\cos(\theta)] \end{aligned}$$

$$= L_F\{[F_{y,FL} + F_{y,FR}]\cos(S_W) + [F_{x,FL} + F_{x,FR}]\sin(S_W)\} - L_R[F_{y,RL} + F_{y,RR}]$$
$$+ \frac{d_F}{2}\{[F_{y,FL} - F_{y,FR}]\sin(S_W) + [F_{x,FR} - F_{x,FL}]\cos(S_W)\} + \frac{d_R}{2}[F_{x,RR} - F_{x,RL}]$$
$$+ \sum_{j=L,R}\{F_{x,Tj}[c\sin(\theta) - y_{Tj}] + F_{y,Tj}[-c\cos(\theta) - L_{TOT,T}]\} \quad (13)$$

where L_F is the front semi-wheelbase of the car; and d_F and d_R are its front and rear track widths.

- Hitch dynamics equation

$$J_3\ddot{\theta} - J_2(\theta)\ddot{\psi} + m_T L_{F,T}\cos(\theta)\left[\dot{V}_y + V_x\dot{\psi}\right] + m_T L_{F,T}\sin(\theta)\left\{\dot{V}_x - \dot{\psi}[V_y - c\dot{\psi}]\right\}$$
$$= \sum_{j=L,R}[F_{x,Tj}y_{Tj} + F_{y,Tj}L_{TOT,T}] - \Gamma\dot{\theta} \quad (14)$$

The wheel moment balance equations, which were obtained outside the Lagrange formulation because of their simplicity, are:

$$\begin{aligned} I_{w,F}\dot{\omega}_{Fj} &= \tau_{m,Fj} - \tau_{b,Fj} - F_{x,Fj}R - fF_{z,Fj}R \\ I_{w,R}\dot{\omega}_{Rj} &= -\tau_{b,Rj} - F_{x,Rj}R - fF_{z,Rj}R \\ I_{w,T}\dot{\omega}_{Tj} &= -\tau_{b,Tj} - F_{x,Tj}R - fF_{z,Tj}R \end{aligned} \quad (15)$$

where $I_{w,F}$, $I_{w,R}$ and $I_{w,T}$ are the wheel mass moments of inertia on the front and rear axles of the car, and the trailer axle; $\tau_{m,Fj}$ is the electric powertrain torque at the wheel, which is present only on the front axle of the car given the front-wheel-drive architecture of the vehicle; $\tau_{b,ij}$ is the braking torque, which, in this study focused on traction conditions, is considered as an external input; $F_{z,ij}$ is the vertical tyre load; R is the laden wheel radius; and f is the rolling resistance coefficient. In (11)–(15), the longitudinal and lateral tyre forces are calculated with the Pacejka Magic Formula version in [43], starting from the tyre slip ratio, slip angle and vertical load, and including consideration of combined slip effects. The slip angles of the car (α_{ij}, with $i = F, R$) and the trailer (α_{Tj}) are given by:

$$\begin{aligned} \alpha_{ij} &= \tan^{-1}\left(\frac{V_y + x_{ij}\dot{\psi}}{V_x - y_{ij}\dot{\psi}}\right) - k_1 S_W, \text{ for } i = F, R, \text{ where } \begin{cases} k_1 = 1 & \text{if} \quad i = F \\ k_1 = 0 & \text{if} \quad i = R \end{cases} \\ \alpha_{Tj} &= \tan^{-1}\left(\frac{V_x\sin(\theta) + V_y\cos(\theta) - c\dot{\psi}\cos(\theta) - L_{TOT,T}[\dot{\psi} - \dot{\theta}]}{V_x\cos - V_y\sin(\theta) + c\dot{\psi}\sin(\theta) - y_{Tj}[\dot{\psi} - \dot{\theta}]}\right) \end{aligned} \quad (16)$$

The vertical tyre loads, $F_{z,ij}$, are obtained as the sum of the static loads, $F_{z,s,ij}$, the longitudinal load transfers, $\Delta F_{z,long,i}$, and the lateral load transfers, $\Delta F_{z,lat,i}$:

$$F_{z,ij} = F_{z,s,ij} + \Delta F_{z,long,i} + k_2\Delta F_{z,lat,i}, \text{ where } k_2 = \begin{cases} 1 & if \quad j = L \\ -1 & if \quad j = R \end{cases} \quad (17)$$

$\Delta F_{z,long,i}$ and $\Delta F_{z,lat,i}$ are computed through steady-state equations based on the system geometry and roll stiffness distribution, and are considered to be directly proportional to the measured longitudinal and lateral accelerations of the towing car, $a_{x,meas}$ and $a_{y,meas}$,

and the estimated longitudinal and lateral accelerations of the centre of gravity of the trailer, $a_{x,T}$ and $a_{y,T}$, which are assumed constant to the purpose of the NMPC prediction. Hence, also the resulting $\Delta F_{z,long,i}$ and $\Delta F_{z,lat,i}$ remain constant along the prediction horizon. In particular, the terms $\Delta F_{z,lat,i}$, which are especially relevant in the considered manoeuvres, are computed as:

$$\begin{aligned}\Delta F_{z,lat,F} &= -\left\{\frac{ma_{y,meas}L_R}{L_{TOT}} - \left[m_T a_{x,T}\sin(\theta) + \frac{m_T a_{y,T} L_{R,T}}{L_{TOT,T}}\cos(\theta)\right]\frac{c-L_R}{L_{TOT}}\right\}\frac{RCH}{d_F} \\ &\quad - \frac{K_{roll,F}\left\{ma_y H_{roll} + \left[m_T a_{x,T}\sin(\theta) + \frac{m_T a_{y,T} L_{R,T}}{L_{TOT,T}}\cos(\theta)\right][H_{hitch} - RCH]\right\}}{d_F[K_{roll,F} + K_{roll,R}]}\end{aligned} \tag{18}$$

$$\begin{aligned}\Delta F_{z,lat,R} &= -\left\{\frac{ma_{y,meas}L_F}{L_{TOT}} + \left[m_T a_{x,T}\sin(\theta) + \frac{m_T a_{y,T} L_{R,T}}{L_{TOT,T}}\cos(\theta)\right]\frac{c+L_F}{L_{TOT}}\right\}\frac{RCH}{d_R} \\ &\quad - \frac{K_{roll,R}\left\{ma_y H_{roll} + \left[m_T a_{x,T}\sin(\theta) + \frac{m_T a_{y,T} L_{R,T}}{L_{TOT,T}}\cos(\theta)\right][H_{hitch} - RCH]\right\}}{d_R[K_{roll,F} + K_{roll,R}]}\end{aligned} \tag{19}$$

$$\Delta F_{z,lat,T} = \frac{m_T a_{y,T} L_{R,T}}{d_T L_{TOT,T}} H_{hitch} - \frac{m_T a_{y,T} H_{CG,T}}{d_T} \tag{20}$$

where RCH is the roll centre height of the suspensions of the car, for which the roll axis is approximated as horizontal; H_{roll} is the distance between the centre of gravity and roll axis of the car; $H_{CG,T}$ is the centre of gravity height of the trailer; H_{hitch} is the height of the hitch joint from the ground; and $K_{roll,F}$ and $K_{roll,R}$ are the front and rear roll stiffness of the suspensions of the car.

(11)–(20), together with the definitions of the slip ratios and the tyre model, were rearranged through symbolic computation software (Maple) into a nonlinear state-space formulation:

$$\dot{X}_S = f(X_S(t), U_C(t)) \tag{21}$$

where X_S is the state vector:

$$X_S = [V_x, V_y, \dot{\psi}, \dot{\theta}, \theta, \omega_{FL}, \omega_{FR}, \omega_{RL}, \omega_{RR}, \omega_{TL}, \omega_{TR}]^T \tag{22}$$

and U_C is the control action vector:

$$U_C = [\tau_{m,FL}, \tau_{m,FR}]^T \tag{23}$$

2.3. Nonlinear optimal control problem formulation

Nonlinear model predictive control is based on the solution of an optimisation problem, in which the discretised internal model, described by the function f_d, is used to predict the future behaviour of the system over a finite prediction horizon, along which the control

actions are obtained to minimise an optimality criterion, i.e. a cost function, while satisfying an assigned set of constraints. Only the control actions computed for the first step of the prediction horizon are applied to the plant, whilst the following control inputs are discarded. Once a new set of states at the next time step is obtained, the whole process is repeated, and new control actions are determined, according to the so-called receding horizon approach [44].

The discrete time formulation of the nonlinear optimal control problem is:

$$\begin{aligned} \min_{U} J(Z(0), U(\cdot)) := \frac{1}{2}\left\{\sum_{k=0}^{N-1}[||Z^k - Z_d^k||_Q^2 + ||U^k||_R^2] + ||Z^N - Z_d^N||_{Q_N}^2\right\} \\ \text{s.t.} \\ X^{k+1} = f_d(X^k, U^k) \\ Z^k = g_d(X^k, U^k) \\ \underline{Z} \leq Z^k \leq \bar{Z} \\ \underline{Z} \leq Z^N \leq \bar{Z} \\ \underline{U} \leq U^k \leq \bar{U} \\ U(\cdot) : [0, N-1] \end{aligned} \tag{24}$$

where J is the cost function; Z is the output vector; U is the control input vector, which includes U_C and the slack variables (defined in the remainder); N is the number of steps of the prediction horizon, which is equal to the control horizon in the considered implementations; the superscript k indicates the discretisation step; Z_d is the vector of desired outputs, which are considered constant along the prediction horizon; g_d is the function that generates the outputs from the states and control inputs; $\underline{Z}$ and $\bar{Z}$ are the lower and upper limits for Z; $\underline{U}$ and $\bar{U}$ are the lower and upper limits for U; and Q, Q_N and R are positive semi-definite weight matrices.

The following subsections 2.4–2.8 provide the details of the considered TV controller formulations based on the general nonlinear optimal control problem in (24).

2.4. Benchmarking TV controller for rigid vehicles (YR_{rig})

This controller, referred to as YR_{rig}, uses the internal model of the rigid vehicle configuration, i.e. it excludes the trailer terms of (11)–(22), and does not consider the presence of the trailer in any aspect of the formulation (hence, it excludes hitch angle feedback). Therefore, in the remainder it is considered as the benchmarking controller. The objective of the formulation is to simultaneously track the desired total powertrain torque demand, $\tau_{m,tot,d}$, set by a dedicated drivability module, and the reference yaw rate, $\dot{\psi}_d$, while limiting the rear axle sideslip angle, α_R, for stability reasons.

The output and reference vectors are defined as:

$$\begin{aligned} Z &= [\tau_{m,tot}, \dot{\psi}, s_\alpha]^T \\ Z_d &= [\tau_{m,tot,d}, \dot{\psi}_d, 0]^T \end{aligned} \tag{25}$$

where $\tau_{m,tot} = \tau_{m,FL} + \tau_{m,FR}$ is the total motor torque demand at the wheels; and s_α, which has zero as reference value, is the slack variable used for imposing the soft constraint on

α_R. (26)–(29) are the constraint formulations:

$$\tau_{m,Fj}^{min} \leq \tau_{m,Fj}^{k} \leq \tau_{m,Fj}^{max} \tag{26}$$

$$s_{\alpha}^{k} \geq 0 \tag{27}$$

$$-\alpha_R^{max}(1+s_{\alpha}^{k}) \leq \alpha_R^{k} \leq \alpha_R^{max}(1+s_{\alpha}^{k}) \tag{28}$$

$$P_{Batt}^{min} \leq P_{Batt}^{k} \leq P_{Batt}^{max} \tag{29}$$

In particular, (26) expresses the constraint in terms of upper and lower bounds on the motor torque demand, defined from the limits of the electric machines and the possible output of an external traction controller; (27) and (28) express the soft constraint on α_R; and (29) deals with the battery power limits, defined by P_{Batt}^{min} and P_{Batt}^{max}. The constraints in (26)–(29) are used also in the other NMPC formulations in Sections 2.5–2.8, in which they are omitted for conciseness.

2.5. TV controller for car–trailer combinations, based on a modified reference yaw rate formulation ($MYR_{d,rig}$)

This formulation, referred to as $MYR_{d,rig}$, is very similar to YR_{rig}, as it uses the internal model of the rigid vehicle. However, when the car tows a trailer, $\dot{\psi}_d$ in (25) is replaced with a modified reference yaw rate, $\dot{\psi}_{dm}$, which is a weighted linear combination of $\dot{\psi}_d$, and the hitch angle error $\Delta\theta = \theta_d - \theta$, with θ_d being kept constant along the prediction horizon:

$$\dot{\psi}_{dm} = \dot{\psi}_d - W_\theta(1-K_\theta)\Delta\theta \tag{30}$$

$\Delta\theta$ has an influence only when it exceeds pre-determined critical thresholds, according to the weighting factor K_θ that modulates the hitch angle correction:

$$K_\theta = \begin{cases} 1 & \text{if} \quad \Delta\theta \in [-\Delta\theta_{th};\, \Delta\theta_{th}] \\ 1 + \left[\frac{K_{\theta,min}-1}{\Delta\theta_{th}-\Delta\theta_{lim}}\right][\Delta\theta_{th} - |\Delta\theta|] & \text{if} \quad \Delta\theta \in [-\Delta\theta_{lim};\, -\Delta\theta_{th}] \cup [\Delta\theta_{th};\, \Delta\theta_{lim}] \\ K_{\theta,min} & \text{if} \quad \Delta\theta \notin [-\Delta\theta_{lim};\, \Delta\theta_{lim}] \end{cases} \tag{31}$$

where $\Delta\theta_{th}$, $\Delta\theta_{lim}$ (with $\Delta\theta_{lim} > \Delta\theta_{th}$) and $K_{\theta,min}$ are tuning parameters. In the first case in (31), the controller tracks only the reference yaw rate of the car, as the hitch angle dynamics are not deemed critical. In the second condition in (31), the controller progressively blends the car yaw rate and hitch angle error contributions, i.e. the reference yaw rate magnitude is increased if the trailer tends to sway toward the external side of the curve with respect to the reference, while the opposite occurs, i.e. $|\dot{\psi}_{dm}| < |\dot{\psi}_d|$, if the trailer tends to rotate to rotate toward the inner side of the turn. In extremely critical conditions, the blending uses $K_{\theta,min}$, which is a small strictly positive value that gives priority to hitch angle tracking, but still allows the TV controller to take into account the steering input by the driver or the automated driving controller also during extreme oscillations of the trailer. Finally, W_θ is a constant gain that provides an extra degree of tuning and addresses the different dimensions of $\dot{\psi}_d$ and $\Delta\theta$.

2.6. TV controller based on the car–trailer model and a hitch angle error constraint ($YR + SC_{HAE}$)

The $YR + SC_{HAE}$ approach uses the car–trailer model in Section 2.2 for the NMPC prediction, and considers a soft constraint on $\Delta\theta$, which is activated only above the specified threshold $\Delta\theta_{lim}$, through a slack variable s_θ, included in the cost function. Therefore, Z and Z_d are:

$$\begin{aligned} Z &= [\tau_{m,tot}, \dot{\psi}, s_\alpha, s_\theta]^T \\ Z_d &= [\tau_{m,tot,d}, \dot{\psi}_d, 0, 0]^T \end{aligned} \tag{32}$$

In addition to those in (26)–(29), the control problem includes the constraints related to s_θ:

$$s_\theta^k \geq 0 \tag{33}$$

$$-\Delta\theta_{lim}(1 + s_\theta^k) \leq \Delta\theta^k \leq \Delta\theta_{lim}(1 + s_\theta^k) \tag{34}$$

where the dynamics of $\Delta\theta$ along the prediction horizon are generated by the prediction model, starting from the measured hitch angle at the current time.

2.7. TV controller based on the car–trailer model and a hitch angle error function ($YR + HAE_{fun}$)

The $YR + HAE_{fun}$ formulation uses the car–trailer model, and includes the hitch angle error in J, through a continuous deadband-like function, according to which the effect of $\Delta\theta$ is progressively taken in account only if the predicted hitch angle error exceeds a pre-determined threshold. Z and Z_d are defined as:

$$\begin{aligned} Z &= [\tau_{tot}, \dot{\psi}, \Delta\theta_c, s_\alpha]^T \\ Z_d &= [\tau_{tot,d}, \dot{\psi}_d, 0, 0]^T \end{aligned} \tag{35}$$

in which $\Delta\theta_c$ is the modified hitch angle error, shown in Figure 3 as a function of $\Delta\theta$, and formulated as:

$$\Delta\theta_c = \Delta\theta - \Delta\theta_{th} \tanh\left(\frac{\Delta\theta}{\Delta\theta_{th}}\right) \tag{36}$$

where $\Delta\theta_{th}$ is the hitch angle error threshold, which is constant along the prediction horizon, while $\Delta\theta_c$ and $\Delta\theta$ vary according to the prediction model dynamics.

2.8. TV controller based on the car–trailer model and a modified yaw rate error (MYRE)

The *MYRE* approach modifies the yaw rate error $\Delta\dot{\psi} = \dot{\psi}_d - \dot{\psi}$, by substituting it with a weighted linear combination ($\Delta\dot{\psi}_m$) of the yaw rate error and hitch angle error, where the latter has an influence only when it exceeds pre-determined thresholds, as shown in [24].

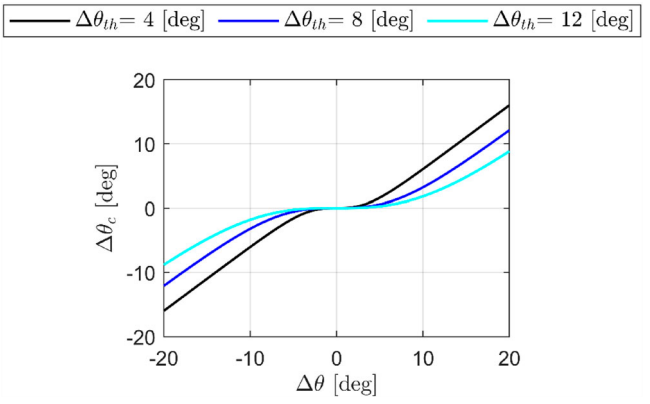

Figure 3. $\Delta\theta_c$ as a function of $\Delta\theta$, for different values of $\Delta\theta_{th}$.

Z and Z_d are defined as:

$$\begin{aligned} Z &= [\tau_{m,tot},\ \Delta\dot{\psi}_m,\ s_\alpha]^T \\ Z_d &= [\tau_{m,tot,d}\,, 0,\ 0]^T \end{aligned} \tag{37}$$

where $\Delta\dot{\psi}_m$ is given by:

$$\Delta\dot{\psi}_m = K_\theta \Delta\dot{\psi} - W_\theta(1 - K_\theta)\Delta\theta \tag{38}$$

with K_θ having been defined in (31).

3. Simulation environment and controller implementation

3.1. Simulation environment

The simulation environment for control system performance assessment consists of the following functional blocks, see Figure 4:

- The driver model, which generates the steering and accelerator pedal inputs, S_W and p_a, according to the considered set of manoeuvres.
- The drivability controller, which outputs the total powertrain torque demand at the vehicle level, $\tau_{m,tot}$, starting mainly from V and p_a.
- The implicit (i.e. online) implementations of the NMPC formulations in Section 2.
- The traction controller, regulating the output torques of the TV controller through a proportional integral (PI) controller, to prevent significant levels of wheel slip in traction. This control function is not described in detail, as it is never active in the selected manoeuvres.
- The high-fidelity nonlinear vehicle simulation model for control system assessment, developed independently from the internal model of the controllers, and characterised by a significantly higher level of accuracy.

The estimators of the relevant vehicle states were not included, as they are covered by a rather extensive literature, e.g. see [25–31].

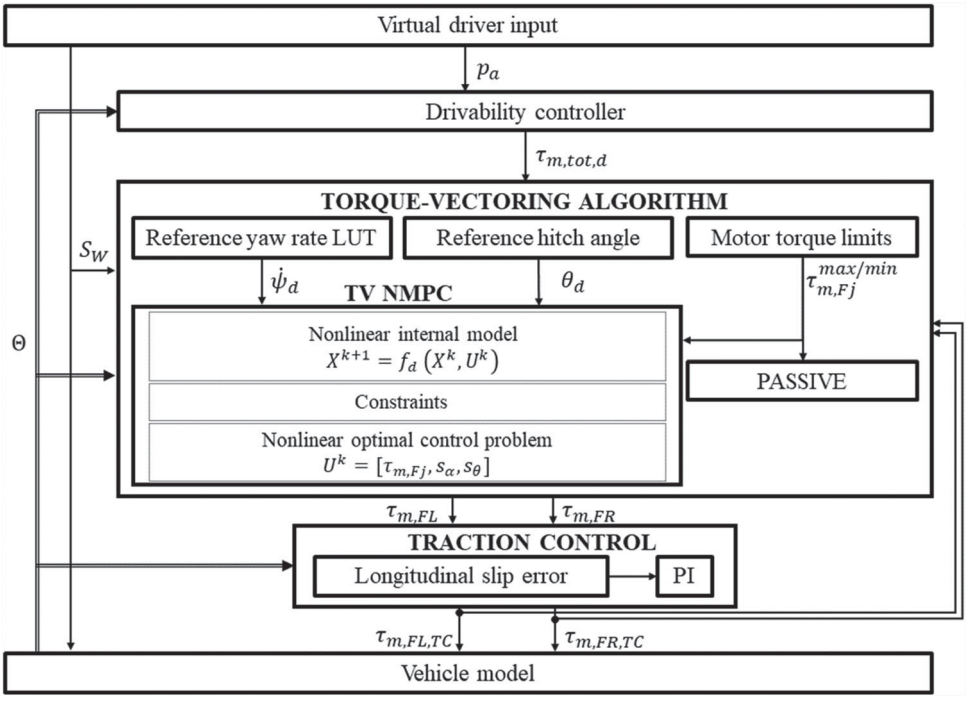

Figure 4. Functional blocks of the simulation environment.

3.2. Case study vehicle and simulation model validation

The case study car is the front-wheel-drive version of the electric sport utility vehicle prototype with individually controlled powertrains, developed in the European projects E-VECTOORC and iCOMPOSE [24], see its main parameters in Table 1. The simulation model for control system assessment evaluates the combination of this car with three production trailers, referred to as trailers A-C in the remainder, with different geometric and inertial properties (the values in the table include the considered payload), to analyse the sensitivity of controller performance to the trailer parameters. The model was implemented in MATLAB-Simulink, and includes the relevant degrees of freedom of the sprung masses and wheels, nonlinear suspension elasto-kinematics, as well as tyre nonlinearities (modelled through the Magic Formula, version 5.2) with relaxation.

The accuracy of the model was verified through experimental tests, carried out at the Lommel proving ground (Belgium), on the electric car prototype towing trailer A, without activation of the TV controller. For example, Figures 5 and 6 report the comparison of the experimental and simulation time profiles of the car yaw rate and trailer hitch angle, along: (i) a single sinusoidal steering test at constant torque demand, with a 40 deg steering wheel angle amplitude and 3 s duration, at an approximately constant speed of 70 km/h; and (ii) a sweep steering test at constant torque demand, with a 25 deg sinusoidal steering wheel input at progressively increasing frequency, at $\sim$90 km/h. The very good match between simulations and experiments, in particular in terms of hitch angle oscillations, confirms that the simulation model can be considered a valid tool for control system assessment.

Table 1. Main car-trailer system parameters.

Symbol	Name and unit	Value Towing car		
m	Mass [kg]	2290		
J_z	Yaw mass moment of inertia [kgm^2]	2761		
L_{TOT}	Wheelbase [m]	2.660		
R	Wheel radius [m]	0.3706		
L_F	Front semi-wheelbase [m]	1.399		
c	Longitudinal distance from CG to hitch joint [m]	2.111		
d_F, d_R	Track width [m]	1.625		
H_{CG}	Centre of gravity height [m]	0.550		
RCH	Roll axis height at the longitudinal coordinate of CG [m]	0.150		
		Trailer A	Trailer B	Trailer C
m_T	Mass [kg]	1400	1000	500
I_T	Yaw mass moment of inertia [kgm^2]	778	646	481
$L_{F,T}$	Hitch joint to trailer centre of gravity distance [m]	2.666	1.961	2.863
$L_{TOT,T}$	Hitch joint to trailer axle distance [m]	2.800	2.300	2.940

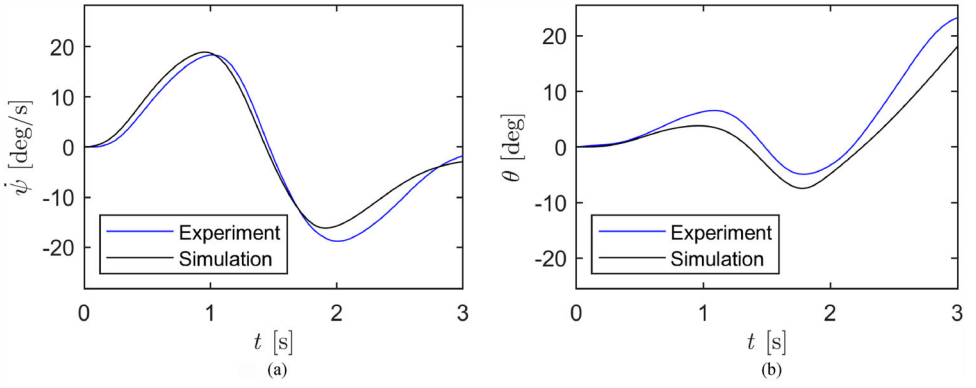

Figure 5. Example of model validation results with trailer A: sinusoidal steering test at $\sim$70 km/h. (a) car yaw rate; and (b) hitch angle.

3.3. Real-time implementation of the controllers

The controllers in Sections 2.4–2.8 were implemented in Simulink through the ACADO toolkit [39], including Gauss–Newton iteration algorithms for fast NMPC with constraints. The selected solver parameters are: multiple shooting discretization method, second-order Runge Kutta integrator, and qpOASES solver.

Moreover, to demonstrate their real-time capability, all proposed controllers were run in real-time on a rapid control prototyping unit, i.e. a dSPACE MicroAutoBox II 1401/1513, with an IBM 900 MHz processor and 16 Mb flash memory, see Figure 7. Given the reduced number of prediction steps to achieve computationally efficient NMPC implementations, the specific dynamic system cannot be considered to be operating in steady-state conditions at the end of the prediction horizon [45], and therefore the controllers have the same number of steps for the prediction and control horizons. For real-time implementation, the controller sampling time T_s, which is coincident with the implementation time, was set to 20 ms, with 2 optimisation steps, which corresponds to a 40 ms prediction horizon. The discretization time of the internal model was set to 4 ms, which ensures numerical

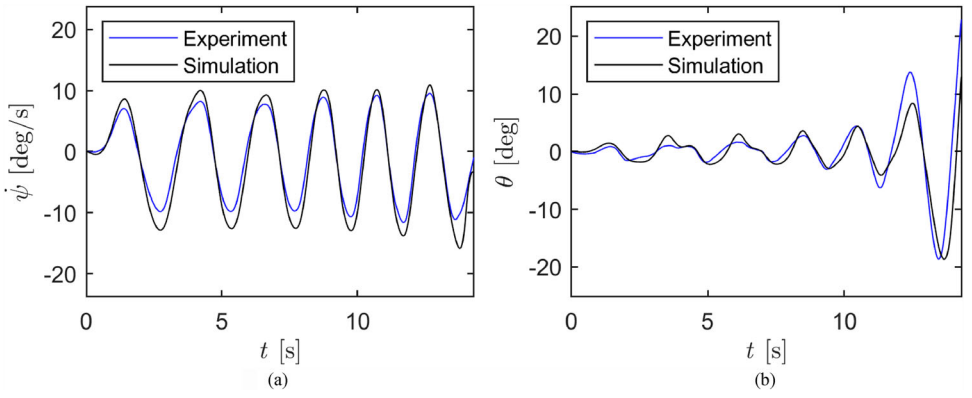

Figure 6. Example of model validation results with trailer A: sweep steering test at ∼90 km/h. (a) car yaw rate; and (b) hitch angle.

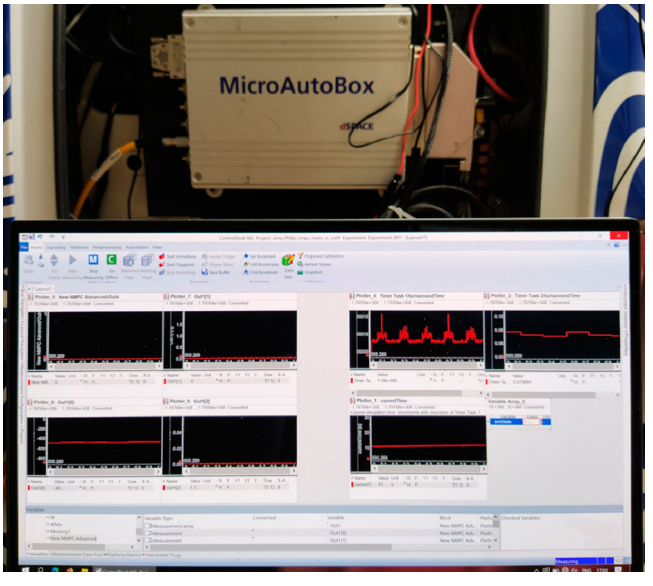

Figure 7. Real-time implementation set-up for the proposed NMPC configurations.

stability without significantly affecting the computational time. Unless otherwise specified, the results of the following sections are obtained with this controller parametrisation.

3.4. Controller tuning routine

The weights related to common cost function terms among all considered controllers (i.e. the weights related to $\tau_{m,tot}$, $\dot{\psi}$, $\tau_{m,FL}$, $\tau_{m,FR}$, and s_α) were selected to be the same across all controllers, and to provide good performance in case of rigid vehicle operation, or articulated vehicle operation along manoeuvres with limited hitch angle dynamics. The cost function weights and calibration parameters that are specific to each controller (see Table 2) were optimised through the automated routine described in this section, to achieve a fair assessment.

The routine runs the simulation model for control system assessment, including the controllers, along a typical critical test (indicated as manoeuvre I in the remainder) for trailer dynamics evaluation, namely a single sinusoidal steering manoeuvre with a 50 deg steering wheel angle amplitude and 3 s duration, from an initial speed of 70 km/h, at a constant 200 Nm wheel torque demand, carried out with trailer A. The main features and tuning parameters of each controller are summarised in Table 2, where W_{s_θ} and $W_{\Delta\theta_c}$ are the weights associated with the hitch angle slack variable (33) and hitch angle error function (36), within the controller cost function (24). Given the rather limited number of tuning parameters of each controller, a brute force algorithm was used to cover the whole parameter space in Table 2, according to the following optimisation problem:

$$\begin{aligned} J^*_{KPI} &= \min_{P_{opt}} J_{KPI}|_{t_i}^{t_f} \\ \text{s.t. } P_{LB} &\leq P_{opt} \leq P_{UB} \end{aligned} \tag{39}$$

where P_{LB} and P_{UB} include the lower and upper bounds of the tuning parameters; P_{opt} is the optimal value of the parameter vector; t_i and t_f are the initial and the final times of the relevant part of the test; and J^*_{KPI} is the optimal value of the cost function J_{KPI}, which is given by the weighted sum of multiple non-dimensional key performance indicators (KPIs):

$$J_{KPI} = W_1 RMSE_{\Delta\dot{\psi}} + W_2 RMSE_{\Delta\theta^*} + W_3 \alpha_R^{max} + W_4 \theta^{max} + W_5 IACA \tag{40}$$

where W_{1-5} are the weights for the individual indicators ($W_1 = 0.3$, $W_2 = 0.35$, $W_3 = 0.10$, $W_4 = 0.20$, and $W_5 = 0.05$ in the specific implementation).

The terms in (40) are:

- The root-mean-square value of the yaw rate error:

$$RMSE_{\Delta\dot{\psi}} = \frac{\sqrt{\frac{1}{t_f - t_i}\int_{t_i}^{t_f} \left[\dot{\psi}_d(t) - \dot{\psi}(t)\right]^2 dt}}{M_{\Delta\dot{\psi}}} \tag{41}$$

Table 2. Features of the implemented controllers and respective tuning parameters.

Controller	Internal model	Description	$P_{LB} \leq P_{opt} \leq P_{UB}$
YR_{rig}	Rigid vehicle	Yaw rate tracking for the rigid vehicle	–
$MYR_{d,rig}$	Rigid vehicle	Reference yaw rate given by the weighted linear combination of the car yaw rate and hitch angle error	$-100\ \text{s}^{-1} \leq W_\theta \leq -0.9\ \text{s}^{-1}$ $0.1 \leq K_{\theta,min} \leq 0.9$ $3\ \text{deg} \leq \Delta\theta_{lim} \leq 10\ \text{deg}$ $2 \leq W_{s_\theta} \leq 1000$
$YR + SC_{HAE}$	Car-trailer	Yaw rate tracking and soft constraint on hitch angle error	$3\ \text{deg} \leq \Delta\theta_{lim} \leq 10\ \text{deg}$
$YR + HAE_{fun}$	Car-trailer	Yaw rate tracking and hitch angle error control through continuous function	$200 \leq W_{\Delta\theta_c} \leq 4000$
$MYRE$	Car-trailer	Control error given by the weighted linear combination of the yaw rate error and hitch angle error	$-100\ \text{s}^{-1} \leq W_\theta \leq -1\ \text{s}^{-1}$ $0.1 \leq K_{\theta,min} \leq 1$ $3\ \text{deg} \leq \Delta\theta_{lim} \leq 10\ \text{deg}$

where $M_{\Delta\dot{\psi}}$ is a normalisation factor, expressed as the maximum expected value of the performance indicator, i.e. $RMSE_{\Delta\dot{\psi}}$. The same criterion was used for the selection of the normalisation factors of the other indicators, i.e. $M_{\Delta\theta^*}$, $M_{\alpha_R^{max}}$, and $M_{\theta^{max}}$, and M_{IACA}.

- The root-mean-square value of the hitch angle error, to assess the level of trailer sway:

$$RMSE_{\Delta\theta^*} = \frac{\sqrt{\frac{1}{t_f - t_i}\int_{t_i}^{t_f}[\Delta\theta^*]^2 dt}}{M_{\Delta\theta^*}} \tag{42}$$

$$\Delta\theta^* = \begin{cases} |\theta_d(t) - \theta(t)| - \Delta\theta_{bound} & \text{if} \quad |\theta_d(t) - \theta(t)| > \Delta\theta_{bound} \\ 0 & \text{if} \quad |\theta_d(t) - \theta(t)| \leq \Delta\theta_{bound} \end{cases} \tag{43}$$

where $\Delta\theta_{bound} = 7$ deg is the hitch angle error bound of the deadband function in (43).

- The maximum rear axle sideslip angle (in absolute value), to assess the stability of the car:

$$\alpha_R^{max} = \frac{\max|\alpha_R|}{M_{\alpha_R^{max}}} \tag{44}$$

- The maximum hitch angle (in absolute value), which shows the most critical condition of the vehicle combination:

$$\theta^{max} = \frac{\max|\theta|}{M_{\theta^{max}}} \tag{45}$$

- The integral of the absolute value of the control action, *IACA*, given by the front powertrain torque difference, which evaluates the control effort:

$$IACA = \frac{\frac{1}{t_f - t_i}\int_{t_i}^{t_f}|\tau_{m.FL}(t) - \tau_{m,FR}(t)|dt}{M_{IACA}} \tag{46}$$

To analyse the performance of the controllers in a wider range of conditions, in the remainder J_{KPI} and the respective individual performance indicators have been calculated also for a second test, referred to as manoeuvre II, i.e. a prolonged sinusoidal steering manoeuvre at a constant steering input frequency of 0.67 Hz, a 65 deg steering wheel angle amplitude, and a $\sim$25 s duration, from an initial speed of 70 km/h, with a constant 200 Nm wheel torque demand. The simulations are stopped if the hitch angle reaches a critical value of 45 deg.

4. Results

For the vehicle combination with trailer A and manoeuvres I and II, Figures 8 and 9 show the time histories of the car yaw rate, hitch angle error, rear axle sideslip angle, and direct yaw moment control action, the latter calculated as:

$$M_z = \frac{[\tau_{m,FL} - \tau_{m,FR}]d_F}{2R} \tag{47}$$

In addition to the considered controlled configurations, the figures include the response of the Passive configuration, i.e. without TV control, which becomes unstable in both tests,

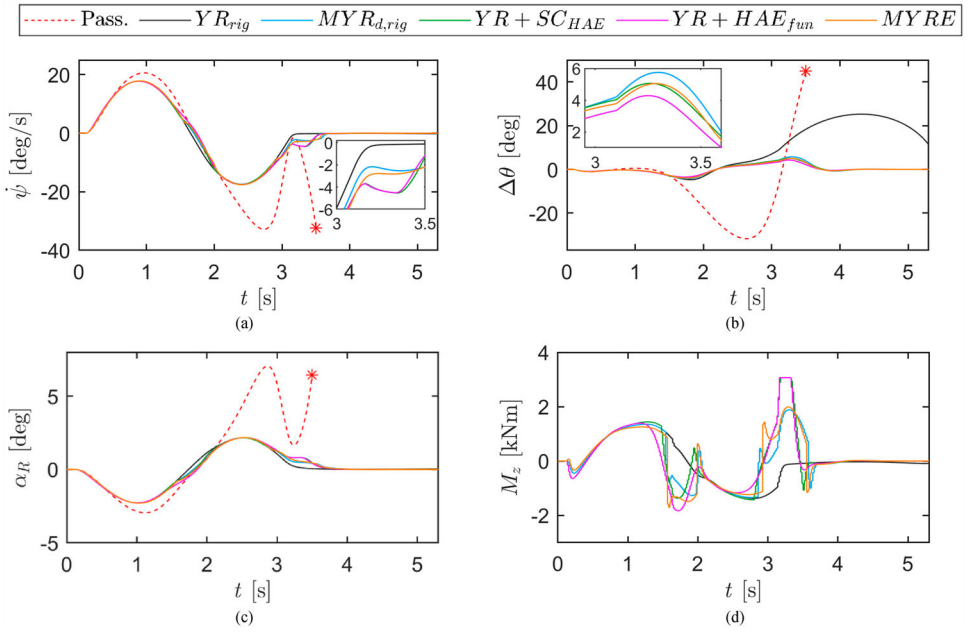

Figure 8. Single sinusoidal steering test (manoeuvre I) with trailer A: (a) car yaw rate; (b) hitch angle error; (c) rear axle sideslip angle; and (d) direct yaw moment control action.

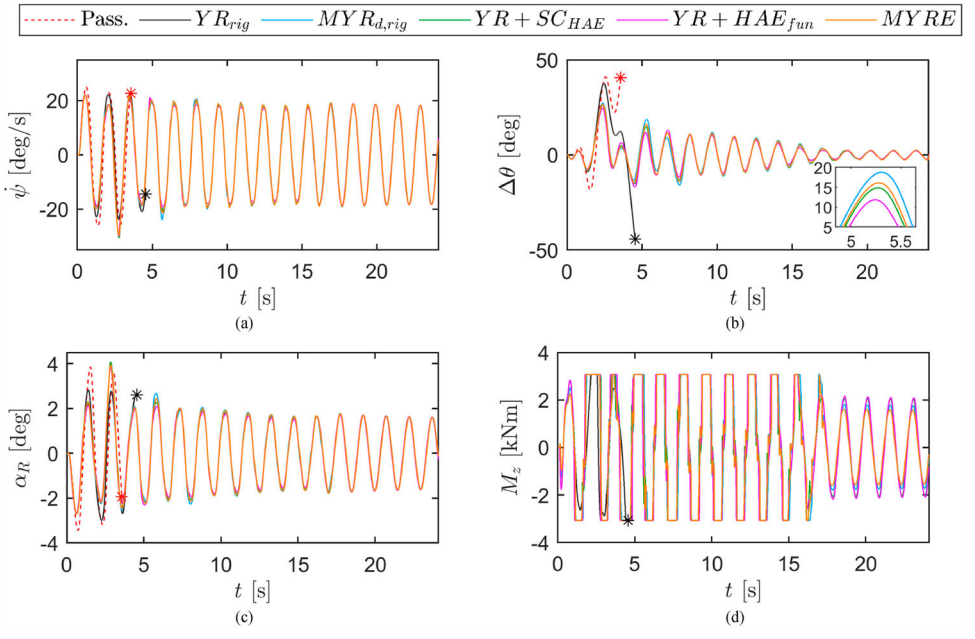

Figure 9. Prolonged sinusoidal steering test (manoeuvre II) with trailer A: (a) car yaw rate; (b) hitch angle error; (c) rear axle sideslip angle; and (d) direct yaw moment control action.

i.e. the simulation is stopped as θ reaches the critical level of 45 deg. In these extreme manoeuvres, the baseline TV configuration, YR_{rig}, which neglects the hitch angle aspects, although behaving better than the passive vehicle, cannot manage to restrain $\Delta\theta$ within

safe limits, i.e. the hitch angle error has a $\sim$25 deg peak amplitude in manoeuvre I, while in manoeuvre II the simulation has to be stopped because of the unstable hitch angle dynamics. Interestingly, all formulations including the hitch angle error contribution show desirable hitch dynamics, with performance differences that are visible only in the zoomed plots in Figure 8(b) and Figure 9(b).

For the single sinusoidal test, Figure 8(a) highlights that in the configurations with hitch angle feedback the car maintains a negative car yaw rate for $>$ 0.5 s after the steering angle is brought back to zero at the end of the manoeuvre, because of the direct yaw moment required to correct trailer sway. In general, direct hitch angle control implies an increase of the M_z control action, see the profiles in Figure 8(d), in which $YR + SC_{HAE}$ and $YR + HAE_{fun}$ reach the yaw moment saturation value imposed by the specific electric motors.

In the prolonged sinusoidal steering test, $YR + SC_{HAE}$ and $YR + HAE_{fun}$ show the best results in terms of hitch angle error limitation, see Figure 9(b). Among the configurations based on feedback hitch angle control, the highest hitch angle error peaks are associated with $MYR_{d,rig}$, as a consequence of its simpler internal model, see the comparison with the *MYRE* formulation, which, although also using a hitch angle based yaw rate correction, considers the vehicle combination dynamics. The control action profile in Figure 9(d) is rather similar for all the hitch angle control configurations, and, given the rather extreme nature of the manoeuvre, M_z reaches its saturation value during each trailer oscillation cycle until $\sim$17.5 s. Afterwards, the marginal vehicle speed reduction caused by the lateral tyre slip power losses makes the manoeuvre less critical, and thus requires less intense direct yaw moments. In the specific test, the M_z peaks tend to limit the magnitude of the yaw rate of the car, and thus to reduce the trailer sway toward the inner side of the vehicle trajectory.

For each controller, Table 3 reports the values of the performance indicators and cost function defined in Section 3.4 along the two considered manoeuvres, performed with the car towing trailers A-C. To evaluate the controller robustness with respect to the variation of trailer parameters, for trailers B and C all controller tunings, including the internal model parameters, are kept constant and equal to those for trailer A. Interestingly, because of its higher mass and yaw moment of inertia, trailer A tends to originate the most critical results, and the NMPCs tuned for trailer A provide desirable performance also with trailers B and C, despite the significant difference in trailer parameters (e.g. the mass of trailer C is approximately one third of the mass of trailer A). The important conclusion is that the model-based hitch angle controllers should be tuned for the most critical trailer parametrisation, and then the resulting controller performance will be acceptable for a very wide range of trailer parameters. The J_{KPI} values across all trailer configurations, as well as the other performance indicators, and in particular $RMSE_{\Delta\theta^*}$ and $|\theta^{max}|$, highlight the good performance of $YR + SC_{HAE}$ and $YR + HAE_{fun}$, i.e. the feedback hitch angle controller formulation should directly consider the hitch angle error, and use a prediction model with trailer dynamics. While in absence of significant hitch angle dynamics excitation, the controllers using the prediction model for the car–trailer tend to enhance the car yaw rate tracking performance in comparison with the benchmarking YR_{rig}, see manoeuvre I with trailer B, in presence of significant hitch angle dynamics, the hitch control stabilisation effort can marginally increase $RMSE_{\Delta\dot{\psi}}$, see manoeuvre I with trailer A, even if in most cases the hitch angle and yaw rate tracking performances concurrently improve.

Table 3. Key performance indicators associated with the passive vehicle and the vehicle with the real-time (RT) implementations of the proposed NMPCs, with trailers A-C, and with the NMPCs with longer prediction horizon (LPH), applied to trailer A.

		Manoeuvre	Pass.	YR_{rig}	$MYR_{d,rig}$	$YR + SC_{HAE}$	$YR + HAE_{fun}$	$MYRE$
Trailer A (RT)								
$RMSE_{\Delta\dot{\psi}}$	[deg/s]	*I*	9.90*	1.11	1.61	1.82	2.03	1.82
		II	9.87*	4.49*	2.31	2.22	2.13	2.41
$RMSE_{\Delta\theta*}$	[deg]	*I*	13.00*	9.27	0.00	0.00	0.00	0.00
		II	16.70	13.37*	3.44	3.08	2.83	3.18
$\lvert\alpha_R^{max}\rvert$	[deg]	*I*	7.06*	2.29	2.29	2.27	2.27	2.29
		II	3.86*	3.00*	3.88	4.08	3.85	3.96
$\lvert\theta^{max}\rvert$	[deg]	*I*	45.00*	25.25	5.89	5.44	5.13	5.65
		II	45.00*	45.00*	27.22	26.30	25.03	26.58
IACA	[Nm]	*I*	–	251	295	318	305	324
		II	–	825*	900	920	962	843
J_{KPI}	[-]	*I*	/	0.56	0.15	0.15	0.15	0.15
		II	/	/	0.57	0.55	0.53	0.56
Trailer B (RT)								
$RMSE_{\Delta\dot{\psi}}$	[deg/s]	*I*	5.29*	1.28	1.28	1.16	1.23	1.38
		II	5.97	2.91	2.12	2.22	2.33	2.37
$RMSE_{\Delta\theta*}$	[deg]	*I*	8.63*	0.00	0.00	0.00	0.00	0.00
		II	6.44	5.02	3.15	2.82	2.66	2.98
$\lvert\alpha_R^{max}\rvert$	[deg]	*I*	3.04*	2.36	2.36	2.34	2.34	2.37
		II	3.76	2.97	2.71	2.68	2.69	2.70
$\lvert\theta^{max}\rvert$	[deg]	*I*	45.00*	3.22	3.22	3.21	3.21	3.22
		II	40.33	31.88	23.70	22.18	21.88	22.92
IACA	[Nm]	*I*	–	262	262	280	269	248
		II	–	622	917	966	984	851
J_{KPI}	[-]	*I*	/	0.11	0.11	0.11	0.11	0.11
		II	–	0.64	0.51	0.48	0.48	0.49
Trailer C (RT)								
$RMSE_{\Delta\dot{\psi}}$	[deg/s]	*I*	2.71	0.98	0.98	0.88	0.88	1.07
		II	8.96*	2.82	1.86	1.73	1.70	2.03
$RMSE_{\Delta\theta*}$	[deg]	*I*	0.00	0.00	0.00	0.00	0.00	0.00
		II	17.58*	4.39	2.21	1.84	1.79	2.12
$\lvert\alpha_R^{max}\rvert$	[deg]	*I*	2.84	2.24	2.24	2.23	2.23	2.25
		II	3.98*	2.80	3.14	2.82	2.93	3.17
$\lvert\theta^{max}\rvert$	[deg]	*I*	5.03	3.94	3.94	3.92	3.92	3.93
		II	45.00*	26.30	21.19	19.72	20.23	21.07
IACA	[Nm]	*I*	–	262	262	280	269	248
		II	–	622	917	966	984	851
J_{KPI}	[-]	*I*	–	0.11	0.11	0.11	0.11	0.11
		II	/	0.55	0.46	0.42	0.43	0.45
Trailer A (LPH)								
$RMSE_{\Delta\dot{\psi}}$	[deg/s]	*I*	9.90*	1.31*	1.26	2.17	2.10	1.37
		II	9.87*	8.08*	5.98	3.30	3.21	4.24
$RMSE_{\Delta\theta*}$	[deg]	*I*	13.00*	15.70*	0.00	0.00	0.00	0.00
		II	16.70	19.85*	6.74	1.49	1.57	4.10
$\lvert\alpha_R^{max}\rvert$	[deg]	*I*	7.06*	2.31*	2.31	2.29	2.29	2.29
		II	3.86*	3.57*	5.28	2.90	3.00	5.75
$\lvert\theta^{max}\rvert$	[deg]	*I*	45.00*	45.00*	6.51	5.03	5.18	6.19
		II	45.00*	45.00*	35.96	19.44	19.89	29.57
IACA	[Nm]	*I*	–	/	275	299	252	261
		II	–	/	699	746	756	793
J_{KPI}	[-]	*I*	/	/	0.15	0.15	0.14	0.15
		II	/	/	0.80	0.43	0.43	0.65

∗: the hitch angle reaches the critical threshold at which the simulation is automatically interrupted.
-: value not calculated.
/: simulation interrupted; value not calculated.

To appreciate the trade-off between yaw rate tracking and hitch angle stabilisation, Figure 10(a) plots the trailer sway mitigation improvement with respect to YR_{rig}, expressed through $I_{RMSE,\Delta\theta^*}$, as a function of the yaw rate tracking improvement, measured by $I_{RMSE,\Delta\dot{\psi}}$. For each controller, manoeuvre and trailer, $I_{RMSE,\Delta\theta^*}$ and $I_{RMSE,\Delta\dot{\psi}}$ are defined as:

$$I_{RMSE,\Delta\theta^*} = \begin{cases} 100\dfrac{RMSE^{YR_{rig}}_{\Delta\theta^*} - RMSE^{CC}_{\Delta\theta^*}}{RMSE^{Pass}_{\Delta\theta^*}} & \text{if} \quad RMSE^{Pass}_{\Delta\theta^*} > 0 \\ 0 & \text{if} \quad RMSE^{Pass}_{\Delta\theta^*} = 0 \end{cases} \tag{48}$$

$$I_{RMSE,\Delta\dot{\psi}} = 100\frac{RMSE^{YR_{rig}}_{\Delta\dot{\psi}} - RMSE^{CC}_{\Delta\dot{\psi}}}{RMSE^{Pass}_{\Delta\dot{\psi}}} \tag{49}$$

where the superscript 'YR_{rig}' highlights that the indicator is computed for the benchmarking YR_{rig} set-up; the superscript '*CC*' indicates the considered controller, i.e. the one that is compared with YR_{rig}; and the superscript '*Pass*' refers to the passive configuration. Positive values of $I_{RMSE,\Delta\theta^*}$ and $I_{RMSE,\Delta\dot{\psi}}$ mean enhanced performance with respect to YR_{rig}, while negative values correspond to a performance decrease. The performance of the passive vehicle combination is used as normalisation factor in the denominators in (48)-(49), to provide a meaningful order of magnitude of the baseline performance (in some cases the root mean square values of all controlled configurations are so low, that the percentage variations would appear significant even in case of negligible variations of the actual system response). Along manoeuvre I the average $I_{RMSE,\Delta\dot{\psi}}$ values across the three trailers are -1.7%, -0.4%, -1.6% and -4.1%, respectively for $MYR_{d,rig}$, $YR + SC_{HAE}$, $YR + HAE_{fun}$, and *MYRE*, i.e. the yaw rate tracking performance tends to be very marginally reduced than for the benchmarking YR_{rig}, yet it is significantly better than for the passive configuration. However, very importantly, during the same manoeuvre all hitch angle controllers manage to keep $\Delta\theta$ within the defined deadband for the three trailers, while YR_{rig} cannot for trailer A, which causes vehicle instability, and corresponds to $I_{RMSE,\Delta\theta^*} = 71.3\%$. In manoeuvre II, the proposed hitch angle controllers bring concurrent benefits in terms of trailer sway stabilisation and yaw rate tracking for all trailers, with average values of $I_{RMSE,\Delta\theta^*}$ and $I_{RMSE,\Delta\dot{\psi}}$ equal to 33.6% and 15.3% for $MYR_{d,rig}$, 36.8% and 15.6% for $YR + SC_{HAE}$, 38.2% and 15.4% for $YR + HAE_{fun}$, and 35.2% and 13.0% for *MYRE*. These results, together with the generalised reduction of the J_{KPI} values in the table, indicate a major active safety enhancement, which would justify the additional complexity of the hitch angle measurement/estimation for the next generation of stability controllers for car–trailer systems.

To evaluate whether these trends are significantly affected by the NMPC settings, for trailer A Table 3 and Figure 10(b) also include the performance indicators for configurations of the same controllers operating with a longer prediction horizon, i.e. 500 ms, obtained by setting $N = 50$ and 10 ms as update time of the control input. Such configurations are not real-time implementable with the hardware in Figure 7, but could become so with the next generations of automotive micro-controllers, and the related results provide generality to the comparison. Interestingly, while with the baseline set-up the benchmarking YR_{rig} configuration manages to complete manoeuvre I, with $N = 50$ it fails to complete both manoeuvres, while all proposed hitch angle feedback control configurations are always successful. Among them, the best approaches are $YR + HAE_{fun}$ and

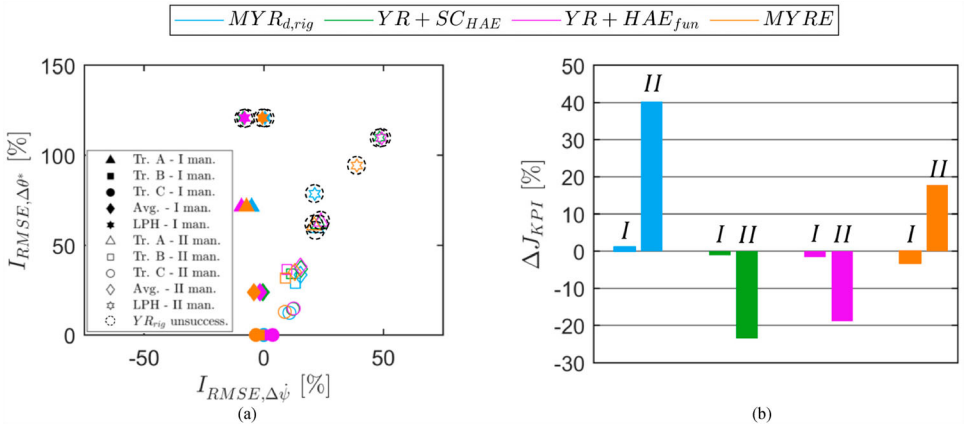

Figure 10. (a) Hitch angle stabilisation improvement of the real-time controller configurations, evaluated through $I_{RMSE,\Delta\theta^*}$, as a function of the car yaw rate tracking improvement, evaluated through $I_{RMSE,\Delta\dot{\psi}}$, with respect to YR_{rig} (the marker associated with 'YR_{rig} unsuccess', highlights the cases in which YR_{rig} cannot complete the test because of trailer instability); and (b) Percentage variation of J_{KPI} for the controller implementations for trailer A with 500 ms prediction horizon, with respect to the corresponding ones with 40 ms prediction horizon.

$YR + SC_{HAE}$, which outperform $MYR_{d,rig}$ and $MYRE$. In general, the extension of the prediction horizon does not automatically ensure a performance improvement, as the driver inputs, i.e. the total wheel torque demand and steering angle, are considered constant along the prediction horizon, which is the typical assumption of model predictive control for vehicle dynamics control, in absence of integration of the predictive controller with the localisation and navigation systems, see the discussion on pre-emptive vehicle stability control in [35]. This is confirmed by Figure 10(b), which plots the percentage variation of J_{KPI}, i.e. ΔJ_{KPI}, for each configuration with the longer prediction horizon, with respect to the corresponding real-time case (a negative value of ΔJ_{KPI} indicates an improvement with the longer prediction horizon). The number of cases with positive and negative ΔJ_{KPI}, and the respective magnitudes, are approximately equivalent, which confirms the effectiveness of the proposed real-time implementations with short prediction horizon.

Similar simulation results, not included in the manuscript, were obtained along lane change manoeuvres from 100 km/h [46], in which the proposed control strategies provide safe behaviour of the car–trailer combination, while the passive vehicle cannot complete the test because of the trailer sway with unstable hitch angle dynamics. The benefits, evident across the range of considered performance indicators, include the reduction the rearward amplification factor (RWA) of the lateral acceleration, defined as the ratio of the maximum value of the lateral acceleration of the centre of gravity of the trailer to that of the car during the test.

5. Conclusions

This study presented four nonlinear model predictive control formulations for the torque-vectoring control of a car towing a single-axle trailer, under the assumption of the availability of measured or estimated hitch angle information. The proposed controllers

target continuous yaw rate control and sideslip angle limitation for the towing car, while limiting the hitch angle dynamics in critical conditions of the vehicle combination. The four novel formulations were implemented in real-time on typical automotive rapid control prototyping hardware, tuned through an optimisation routine using an experimentally validated simulation model, and compared with a benchmarking nonlinear model predictive torque-vectoring controller, along two manoeuvres, carried out with three trailers covering a wide range of parameters. The analysis brought the following conclusions:

- The benchmarking TV controller, YR_{rig}, which tracks only the yaw rate of the car and uses a rigid vehicle model as internal model, does not manage to complete the manoeuvres when it is associated with the heaviest considered trailer. This confirms that dedicated controllers are highly beneficial to the active safety enhancement of vehicle combinations.
- The $MYR_{d,rig}$ controller, which uses the hitch angle error to correct the reference yaw rate of the towing car and only includes the towing car in its internal model, is able to stabilise trailer sway in all considered conditions, and shows desirable yaw rate tracking performance in most cases. Nevertheless, the hitch angle indicators are generally not as good as for the formulations including the car–trailer dynamics in the internal model. $MYR_{d,rig}$ can represent a viable compromise between simplicity of implementation and effectiveness.
- The best performance was obtained with the $YR + HAE_{fun}$ and $YR + SC_{HAE}$ formulations, which include the car–trailer dynamics in their prediction models and use the hitch angle error either in the cost function or in the constraints.
- The least effective configuration among those including the trailer dynamics in the internal model is *MYRE*, which modifies the yaw rate error as a function of the hitch angle error. Nevertheless, the resulting performance is better than for $MYR_{d,rig}$ and especially YR_{rig}.
- The formulations using an internal model of the car–trailer show high level of robustness to the variation of the real trailer parameters with respect to their nominal values used within the prediction model, e.g. the controllers with fixed values of the inertial parameters provided safe performance in emergency conditions for trailer mass values ranging from 500 kg to 1400 kg.
- All proposed controllers are real-time implementable, provided that appropriate parameters, e.g. number of prediction steps and implementation time, are selected. Short prediction horizons do not represent a performance limitation for the specific controllers, as the driver inputs are considered to remain constant along the prediction horizon.

The next steps of this research will focus on the implementation and experimental assessment of the proposed algorithms on real demonstrator vehicles.

Disclosure statement

No potential conflict of interest was reported by the author(s).

Funding

The research leading to these results has received funding from the European Union's Horizon 2020 Research and Innovation Framework Programme under grant agreement no. 824244 (SYS2WHEEL project).

ORCID

Aldo Sorniotti http://orcid.org/0000-0002-4848-058X

References

[1] Darling J, Tilley D, Gao B. An experimental investigation of car-trailer high-speed stability. Proc. Inst. Mech. Eng., Part D: J. Autom. Eng. 2009;223(4):471–484.
[2] Gerum E, Laszlo P, Semsey A, et al. Method for drive stability enhancement of multi-unit vehicles. U.S. Patent No. 5,747,683, 1998.
[3] Mokhiamar O, Abe M. Examination of different models following types of yaw moment control strategy for improving handling safety of a car–caravan combination. Proc. Inst. Mech. Eng.,: Part D: J. Autom. Eng. 2003;217(7):561–571.
[4] Deng W, Kang X. Parametric study on vehicle-trailer dynamics for stability control. SAE Technical Paper 2003-01-1321, 2003.
[5] Fernández MA, Sharp RS. Caravan active braking system-Effective stabilisation of snaking of combination vehicles. SAE Technical Paper 2001-01-3188, 2001.
[6] Plöchl M, Lugner P, Riepl A. Improvements of passenger car-trailer behaviour by a trailer based control system. Veh. Syst. Dyn. 1998;29(S1):438–450.
[7] Sun T, He Y, Ren J. Dynamics analysis of Car-trailer systems with active trailer differential braking strategies. SAE Int. J. Passeng. Cars - Mech. Syst. 2014;7(1):73–85.
[8] Shamim R, Islam M, He Y. A comparative study of active control strategies for improving lateral stability of car-trailer systems. SAE Technical Paper, 2011-01-0959, 2011.
[9] MacAdam C, Hagan M. A simple differential brake control algorithm for attenuating rearward amplification in doubles and triples combination vehicles. Veh. Syst. Dyn. 2002;37(1):234–245.
[10] Milani S, Ünlüsoy YS, Marzbani H, et al. Semitrailer steering control for Improved articulated vehicle manoeuvrability and stability. Nonlin. Eng. 2019;8(1):568–581.
[11] Tabatabaei Oreh SH, Kazemi R, Azadi S. A new desired articulation angle for directional control of articulated vehicles. Proc. Inst. Mech. Eng., Part D: J. Autom. Eng. 2012;226(4):298–314.
[12] Islam M, Ding X, He Y. A closed-loop dynamic simulation-based design method for articulated heavy vehicles with active trailer steering systems. Veh. Syst. Dyn. 2012;50(5):675–697.
[13] He Y, Islam M, Webster T. An Integrated design method for articulated heavy vehicles with active trailer steering systems. SAE Int. J. Passeng. Cars – Mech. Syst. 2010;3(1):158–174.
[14] Keldani M, He Y. Design of an improved robust active trailer steering controller for multi-trailer articulated heavy vehicles using software/hardware-in-the-loop real-time simulations. IAVSD, 2019.
[15] Islam M, He Y. A parallel design optimisation method for articulated heavy vehicles with active safety systems. Int. J. of Heavy Veh.: Syst. 2013;20:327–341.
[16] Vempaty S, He Y, Zhao L. An overview of control schemes for improving the lateral stability of car-trailer combinations. Int. J. Veh. Perf. 2020;6(2):151–199.
[17] Abroshan M, Hajiloo R, Hashemi E, et al. Model predictive-based tractor-trailer stabilisation using differential braking with experimental verification. Veh. Syst. Dyn. 2020;59(8):1–24.
[18] Zhang Y, Khajepour A, Hashemi E, et al. Reconfigurable model predictive control for articulated vehicle stability with experimental validation. IEEE Trans. Transp. Elect. 2020;6(1):308–317.
[19] Wang W, Fan J, Xiong R, et al. Lateral stability control of four wheels independently drive articulated electric vehicle. IEEE Transportation Electrification Conference and Expo, 2016.
[20] [cited 2021 June 21]. Available from: https://media.daimler.com/marsMediaSite/en/instance/ko/The-technology-How-Trailer-Stability-Assist-works.xhtml?oid = 9904516.

[21] Wu H, Nardi F, Chen J, et al. Closed-loop control for trailer sway mitigation. U.S. Patent No. 8,740,317, 2014.
[22] Wu H. Trailer sway mitigation using torque vectoring. U.S. Patent No. 9,061,663, 2015.
[23] AL-KO. Comprehensive catalogue trailer components. Part No. 499 699 B, Edition 06/2021.
[24] Zanchetta M, Tavernini D, Sorniotti A, et al. Trailer control through vehicle yaw moment control: Theoretical analysis and experimental assessment. Mechatronics (Oxf). 2019;64:102282.
[25] Lee Y, Kade A. Trailer articulation angle estimation. U.S. Patent No. 7,904,222, 2008.
[26] Vejlupek J. Trailer Backing-up Assistant using ultrasound sensors based control units to safely back-up the car with trailer. 17th International Conference on Mechatronics – Mechatronika, 2016.
[27] Ahmadi JH, Ghaffari A. Nonlinear estimator design based on extended Kalman filter approach for state estimation of articulated heavy vehicle. Proc. Inst. Mech. Eng., Part K: J. Multi-Body Dyn. 2018;233(2):254–265.
[28] Xu L, Tseng E, Pilutti T, et al. Yaw rate based trailer hitch angle estimation for trailer backup assist. SAE Technical Paper 2017-01-0027, 2017.
[29] Habibnejad Korayem A. State and Parameter Estimation of Vehicle-Trailer Systems [PhD thesis], University of Waterloo, 2021.
[30] Fuchs C, Neuhaus F, Paulus D. 3d pose estimation for articulated vehicles using Kalman-filter based tracking. Pattern Rec. Image An. 2016;26(1):109–113.
[31] Caup L, Salmen J, Muharemovic I, et al. Video-based trailer detection and articulation estimation. IEEE Intelligent Vehicles Symposium, 2013.
[32] Kayacan E, Kayacan E, Ramon H, et al. Learning in centralized nonlinear model predictive control: application to an autonomous tractor-trailer system. IEEE Trans. Contr. Syst. Technol. 2015;23(1):197–205.
[33] Zhang Y, Khajepour A, Ataei A. A universal and reconfigurable stability control methodology for articulated vehicles with any configurations. IEEE Trans. Veh. Technol. 2020;69(4):3748–3759. (early access).
[34] Metzler M, Tavernini D, Gruber P, et al. On prediction model fidelity in explicit nonlinear model predictive vehicle stability control. IEEE Trans. Contr. Syst. Technol. 2020;29(5).
[35] Parra A, Tavernini D, Gruber P, et al. On pre-emptive vehicle stability control. Veh. Syst. Dyn. 2021: 1–26.
[36] Siampis E, Velenis E, Gariuolo S, et al. A real-time nonlinear model predictive control strategy for stabilization of an electric vehicle at the limits of handling. IEEE Trans. Contr. Syst. Technol. 2019;26(6):1982–1994.
[37] Parra A, Tavernini D, Gruber P, et al. On nonlinear model predictive control for Energy-Efficient torque-vectoring. IEEE Trans. Veh. Technol. 2021;70(1):173–188.
[38] Dalboni M, Tavernini D, Montanaro U, et al. Nonlinear model predictive control for integrated energy-efficient torque-vectoring and anti-roll moment distribution. IEEE/ASME Trans. Mechatr. 2021;26(3).
[39] Houska B, Ferreau HJ, Diehl M. ACADO toolkit – an open source framework for automatic control and dynamic optimization. Opt. Contr. Appl. Meth. 2011;32(3):298–312.
[40] De Novellis L, Sorniotti A, Gruber P, et al. Direct yaw moment control actuated through electric drivetrains and friction brakes: Theoretical design and experimental assessment. Mechatronics (Oxf). 2015;26:1–15.
[41] van Zanten AT, Erhardt R, Pfaff G. VDC, the vehicle dynamics control system of Bosch. SAE Technical Paper 950759, 1995.
[42] Genta G, Morello L. The automotive chassis, Volume 2: System Design. Cham: Springer; 2020.
[43] Bakker E, Nyborg L, Pacejka HB. Tyre modelling for use in vehicle dynamics studies. SAE Technical Paper 870421, 1987.
[44] Maciejowski J. Predictive control with constraints. Harlow: Prentice Hall; 2001.
[45] Linder A, Kanchan R, Kennel R, et al. Model-Based predictive control of electric drives. Gottingen: Cuvilier-Verlag; 2012.
[46] International Organization for Standardization (ISO). Road Vehicles – Heavy Commercial Vehicle Combinations and Articulated Buses – Lateral Stability Test Methods. ISO-14791, 2000.